



Acoustic resonant surface: from nearly-total reflection to nearly-total absorption of sound

L. Schwan, O. Umnova

Acoustics Research Center, University of Salford, The Crescent, M5 4WT Salford, U.K.

C. Boutin

E.N.T.P.E., Université de Lyon, LGCB, UMR CNRS 5513, Vaulx-en-Velin, France

H.-C. Shin, S. Taherzadeh and K. Attenborough

The Open University, Engineering and Innovation, Walton Hall, MK7 6AA Milton Keynes, U.K.

Summary

An analytical model is developed to describe the acoustical properties of an array of resonators arranged periodically upon a hard plane surface. The model relies on the scale separation between the lattice constant of the 2D array and the long wavelength of sound at resonance. Due to this, small-scale perturbations of the scattered field remain confined near the resonators within a boundary layer. Two-scale asymptotic homogenization is applied to derive an effective frequency dependent admittance of the surface. It is shown that tuneable surface conditions can be achieved around the resonance frequency, ranging from a nearly total absorption of the acoustical waves to a quasi-total reflection of sound with a phase-shift. The model is validated by comparing its predictions with impedance tube and anechoic chamber measurements and with the Multiple Scattering Theory.

PACS no. 43.60.Fg, 43.20.Rz, 78.67.Pt, 11.80.La

1. Introduction

While surfaces with periodic profiles such as diffusers [1] or air-backed microperforated panels [2] are used widely to control acoustic waves in the middle and high frequency ranges, their application at low frequencies (e.g. below 300 Hz) is hindered by the sizes required for an effective performance. In that range of frequencies, the possibilities of wavefield manipulations have been improved by the use of metamaterials, especially those with inner resonances, e.g. [3, 4, 5].

Here, the concept of microstructured surface is reported with resonant roughness elements arranged periodically on a rigid plane. If the lattice constant of the 2D array is much smaller than the long-wavelength of sound at resonance, it is shown that such a corrugated resonant surface is capable of either total sound absorption or pressure-release reflection, depending on its design. The model developed here is based upon the scale separation between the subwavelength lattice size of the array and the long wavelength of sound at resonance. As a result if it, small-scale multiple interactions between the resonators are confined within

a boundary layer which dictates the effective boundary condition for the long-wavelength field.

In Section 2, the two-scale asymptotic homogenization is applied to describe the resonant array in terms of an effective surface admittance. In Section 3, plane-wave reflection from the array is studied. In Section 4, the analytical model is compared with impedance tube and anechoic chamber measurements. In Section 5, comparisons with Multiple Scattering Theory computations are presented.

2. Homogenization

The resonant surface consists of identical linear resonators arranged in a two-dimensional Σ -periodic array with the lattice constant ℓ , Figure 1. It is placed (contactless) above the plane rigid boundary Γ of the air-filled halfspace (at equilibrium, the density is $\rho_e = 1.2 \text{ kg/m}^3$, the atmospheric pressure $P_e = 1.013 \times 10^5 \text{ Pa}$, the adiabatic constant $\gamma = 1.4$ and the sound speed $c = \sqrt{\gamma P_e / \rho_e} \approx 343.8 \text{ m/s}$). The propagation of acoustic perturbations is studied in the linear harmonic regime at frequencies $f = \omega/2\pi$ (time dependence $e^{-i\omega t}$) close to the eigenfrequency $\omega_o/2\pi$ of the resonators. In that frequency range, the sound wavelength $\lambda = 2\pi c/\omega$ is assumed to be much larger than both the lattice size ℓ of the array and the height $d = \mathcal{O}(\ell)$ of the resonator-induced

(c) European Acoustics Association

roughness. This scale separation is quantified by the small scale parameter $\epsilon = 2\pi\ell/\lambda = \ell\omega/c \ll 1$.

Excited by the long-wavelength acoustic field, the resonators produce the particle velocity \mathbf{V} at their boundary S and act as mutually-interacting secondary sources: the velocity \mathbf{V} is locally Σ -periodic while also varying at the long-wavelength scale. That induces locally-periodic perturbations (pressure p^* and particle velocity \mathbf{v}^*) confined in the vicinity of the resonators, i.e. a boundary layer [6, 7], while the long-wavelength field (pressure p and particle velocity \mathbf{v}) prevails some distance away from the surface.

Both long-wavelength and boundary layer fields satisfy equations (1a,b) of momentum and mass conservation. Their superposition balances the velocity \mathbf{V} on the boundary S (outward normal \mathbf{n}_S) of the resonators, and satisfies the boundary condition on the rigid surface Γ (normal \mathbf{n} pointed at air):

$$i\omega\rho_e\mathbf{v} = \mathbf{grad} p \quad ; \quad i\omega\rho_e\mathbf{v}^* = \mathbf{grad} p^* \quad ; \quad (1a)$$

$$\text{div} \mathbf{v} = i\omega p/\gamma P_e \quad ; \quad \text{div} \mathbf{v}^* = i\omega p^*/\gamma P_e \quad ; \quad (1b)$$

$$(\mathbf{v} + \mathbf{v}^*) \cdot \mathbf{n}_S = \mathbf{V} \cdot \mathbf{n}_S \text{ on } S; \quad (1c)$$

$$(\mathbf{v} + \mathbf{v}^*) \cdot \mathbf{n} = 0 \text{ on } \Gamma. \quad (1d)$$

The two-scale asymptotic homogenization [6, 8] is applied. Two space variables are introduced: \mathbf{x} for the long-wavelength description and $\mathbf{y} = \epsilon^{-1}(\mathbf{x} - \mathbf{x}_\Gamma^0)$ for the local description of the surface over distances $|\mathbf{x} - \mathbf{x}_\Gamma^0| = \mathcal{O}(\ell)$, where $\mathbf{x}_\Gamma^0 \in \Gamma$ is the center of the period Σ . Differentiation is modified accordingly, e.g. $\mathbf{grad} = \mathbf{grad}_x + \epsilon^{-1}\mathbf{grad}_y$ where \mathbf{grad}_x and \mathbf{grad}_y are gradients with respect to \mathbf{x} and \mathbf{y} . Next, the fields are expanded asymptotically in powers of $\epsilon \ll 1$:

$$p(\mathbf{x}) = p^{(0)}(\mathbf{x}) + \epsilon p^{(1)}(\mathbf{x}) + \dots \quad (2a)$$

$$\mathbf{v}(\mathbf{x}) = \mathbf{v}^{(0)}(\mathbf{x}) + \epsilon \mathbf{v}^{(1)}(\mathbf{x}) + \dots \quad (2b)$$

$$p^*(\mathbf{x}_\Gamma^0, \mathbf{y}) = p^{*(0)}(\mathbf{x}_\Gamma^0, \mathbf{y}) + \epsilon p^{*(1)}(\mathbf{x}_\Gamma^0, \mathbf{y}) + \dots \quad (2c)$$

$$\mathbf{v}^*(\mathbf{x}_\Gamma^0, \mathbf{y}) = \mathbf{v}^{*(0)}(\mathbf{x}_\Gamma^0, \mathbf{y}) + \epsilon \mathbf{v}^{*(1)}(\mathbf{x}_\Gamma^0, \mathbf{y}) + \dots \quad (2d)$$

$$\mathbf{V}(\mathbf{x}_\Gamma^0, \mathbf{y}) = \mathbf{V}^{(0)}(\mathbf{x}_\Gamma^0, \mathbf{y}) + \epsilon \mathbf{V}^{(1)}(\mathbf{x}_\Gamma^0, \mathbf{y}) + \dots \quad (2e)$$

At the leading order, the boundary layer fields are governed by the following equations

$$\mathbf{grad}_y p^{*(0)} = \mathbf{0}; \quad (3a)$$

$$\text{div}_y \mathbf{v}^{*(0)} = 0; \quad (3b)$$

$$(\mathbf{v}^{(0)} + \mathbf{v}^{*(0)}) \cdot \mathbf{n}_S = \mathbf{V}^{(0)} \cdot \mathbf{n}_S \text{ on } S; \quad (3c)$$

$$(\mathbf{v}^{(0)} + \mathbf{v}^{*(0)}) \cdot \mathbf{n}_S = 0 \text{ on } \Sigma \subset \Gamma; \quad (3d)$$

$$\mathbf{v}^{*(0)} \rightarrow \mathbf{0} \text{ and } p^{*(0)} \rightarrow 0 \text{ as } \mathbf{y} \cdot \mathbf{n} \rightarrow \infty. \quad (3e)$$

Combining equation (3a) with the evanescence condition (3e) leads to $p^{*(0)} = 0$ i.e. the long-wavelength field $p^{(0)}$ prevails at the leading order, despite the heterogeneous velocity $\mathbf{V}^{(0)}$ and the surface corrugation. Equation (3b) of incompressible flow suggests that the boundary layer has a thickness $\mathcal{O}(\ell)$ otherwise wave propagation would induce compressibility

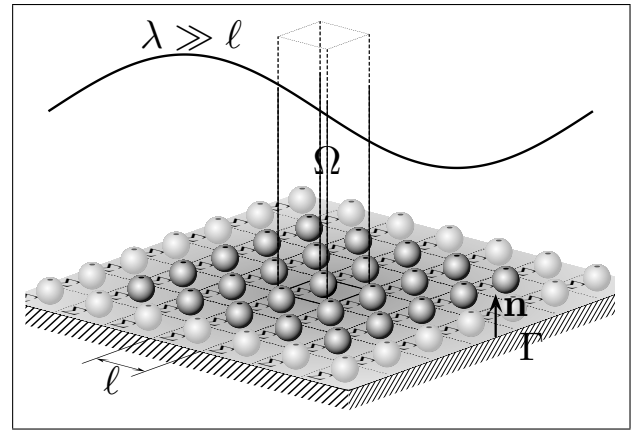


Figure 1. A resonant surface. Σ -periodic arrangement (lattice constant ℓ) of spherical resonators upon a rigid surface and under the scale separation $\lambda \gg \ell$. Representation of the column Ω of air above one period (used in integration).

effects. Applying the divergence theorem and using the Σ -periodicity and evanescence of the boundary layer, the integration of (3b) over the column Ω of air above one period Σ (see Figure 1) leads to the balance of flux:

$$\int_{\Sigma} \mathbf{v}^{*(0)} \cdot \mathbf{n} d\Sigma_y + \oint_S \mathbf{v}^{*(0)} \cdot \mathbf{n}_S dS_y = 0 \quad (4)$$

Besides, since the velocity $\mathbf{v}^{(0)}(\mathbf{x})$ is quasi-uniform at local (\mathbf{y}) scale and since S is a closed volume:

$$\int_{\Sigma} \mathbf{v}^{(0)} \cdot \mathbf{n} d\Sigma_y + \oint_S \mathbf{v}^{(0)} \cdot \mathbf{n}_S dS_y = |\Sigma| \mathbf{v}^{(0)} \cdot \mathbf{n} \quad (5)$$

where $|\Sigma|$ is the area of Σ . Combining equations (4) and (5) with (3d) and (3e), the effective boundary condition is derived for the long-wavelength field:

$$\mathbf{v}^{(0)} \cdot \mathbf{n} = \frac{1}{|\Sigma|} \int_S \mathbf{V}^{(0)} \cdot \mathbf{n}_S dS_y \quad \text{on } \Sigma \subset \Gamma. \quad (6)$$

Since only the flux $q^{(0)} = \int_S \mathbf{V}^{(0)} \cdot \mathbf{n}_S dS$ is significant, at the leading order (a) a local distribution of acoustic moments (flux $q^{(0)} = 0$) results in the boundary condition equivalent to that of a rigid surface; (b) the resonator-induced roughness has no significant effects on the boundary conditions; (c) the knowledge of the exact velocity distribution $\mathbf{V}^{(0)}$ at the resonators' boundary is not required.

In response to the pressure $p_\Gamma^{(0)} = p^{(0)}(\mathbf{x}_\Gamma^0)$, the resonators produce the flux $q^{(0)} = Y_o^{(0)} p_\Gamma^{(0)}$ where $Y_o^{(0)}$ is the frequency-dependent admittance of the resonators at the leading order. Using equation (6), the following boundary condition for the long-wavelength velocity is derived: $\mathbf{v}^{(0)} \cdot \mathbf{n} = \Upsilon^{(0)} p_\Gamma^{(0)}$ on Γ where $\Upsilon^{(0)} = Y_o^{(0)}/|\Sigma|$ is the effective surface admittance of the array.

In the following, superscripts (0) are omitted.

3. Reflection from the surface

The resonant surface can be designed using resonators with a Single Degree Of Freedom (SDOF) characterized by the mass m_o , the stiffness k_o , the weak damping $\xi_o \ll 1$ and the surface area A from where the flux q is emitted. According to Newton's Second Law, $-\omega^2 m_o u_o = -k_o(1 - i2\xi_o \omega/\omega_o)u_o - |A|p_\Gamma$ where $\omega_o = \sqrt{k_o/m_o}$ is the eigenfrequency and u_o the displacement of the mass. The resonators' admittance $Y_o = q/p_\Gamma = -i\omega u_o |A|/p_\Gamma$ is then:

$$Y_o = \frac{|A|^2 \omega_o}{k_o} F(\omega); F(\omega) = \frac{i \frac{\omega}{\omega_o}}{1 - i2\xi_o \frac{\omega}{\omega_o} - \frac{\omega^2}{\omega_o^2}}. \quad (7)$$

The ratio between the resonant surface admittance $\Upsilon = Y_o/|\Sigma|$ and the air admittance $1/\rho_e c$ is given by $\rho_e c \Upsilon = \eta F(\omega)$, where $\eta = |A|^2 \rho_e c \omega_o / (k_o |\Sigma|)$. In the low and high frequency regime ($\omega \ll \omega_o$ and $\omega \gg \omega_o$ respectively), the resonant surface admittance Υ is much smaller than that of the air, hence the surface acts as a rigid boundary. Conversely, at resonance $\omega \rightarrow \omega_o$, the admittance ratio reaches the value $\rho_e c \Upsilon = -\eta/2\xi_o$ which is large provided that $\eta/2\xi_o \gg 1$, hence the surface acts as a pressure release boundary.

To illustrate the effects of the resonant surface admittance, the response of the array to an incident plane wave $p_I \exp(i\omega \mathbf{d}_I \cdot \mathbf{x}/c)$ is studied in the coordinate system $(O, \mathbf{e}_1, \mathbf{e}_2, \mathbf{n})$ where the origin O is at the boundary Γ and the unit vector $\mathbf{e}_2 \in \Gamma$ is in the plane of incidence $(\mathbf{d}_I, \mathbf{n})$ with $\mathbf{d}_I \cdot \mathbf{e}_2 > 0$. The incident wave gives rise to a reflected wave $p_R \exp(i\omega \mathbf{d}_R \cdot \mathbf{x}/c)$ which satisfies Descartes' Laws: \mathbf{d}_R belongs to the plane of incidence and $\mathbf{d}_R \cdot \mathbf{e}_2 = \mathbf{d}_I \cdot \mathbf{e}_2$. Denoting $\theta_I > 0$ the angle of incidence (counted from the normal \mathbf{n} so that $\mathbf{d}_I \cdot \mathbf{n} = -\cos \theta_I$), the resonant surface admittance Υ leads to the pressure reflection coefficient $R = p_R/p_I = [\cos \theta_I + \rho_e c \Upsilon] / [\cos \theta_I - \rho_e c \Upsilon]$ with the following frequency dependence:

$$R = \frac{1 - i2 \left(\xi_o - \frac{\eta}{2 \cos \theta_I} \right) \frac{\omega}{\omega_o} - \frac{\omega^2}{\omega_o^2}}{1 - i2 \left(\xi_o + \frac{\eta}{2 \cos \theta_I} \right) \frac{\omega}{\omega_o} - \frac{\omega^2}{\omega_o^2}} \quad (8)$$

The amplitude of R is sensitive to the resonators' damping (Figure 2): while the use of undamped resonators ($\xi_o = 0$) results in the total reflection of the wave $|R| \equiv 1$ at any frequency, the introduction of weak damping ($\xi_o \ll 1$) leads to a partial reflection $|R| \leq 1$. Far from resonance ($\omega \ll \omega_o$ and $\omega \gg \omega_o$) $R \rightarrow 1$ as if the surface Γ were rigid. However, around the resonance, the reflection coefficient displays a phase shift and a decrease in its amplitude, which depend on the angle of incidence. In particular, the admittance ratio $\rho_e c \Upsilon = -\eta/2\xi_o$ at resonance $\omega \approx \omega_o$ allows vanishing of the reflected wave ($R \rightarrow 0$) if $\cos \theta_I = \eta/2\xi_o \leq 1$. In this case, in the frequency range close to resonance, the surface acts as a totally-absorbing boundary.

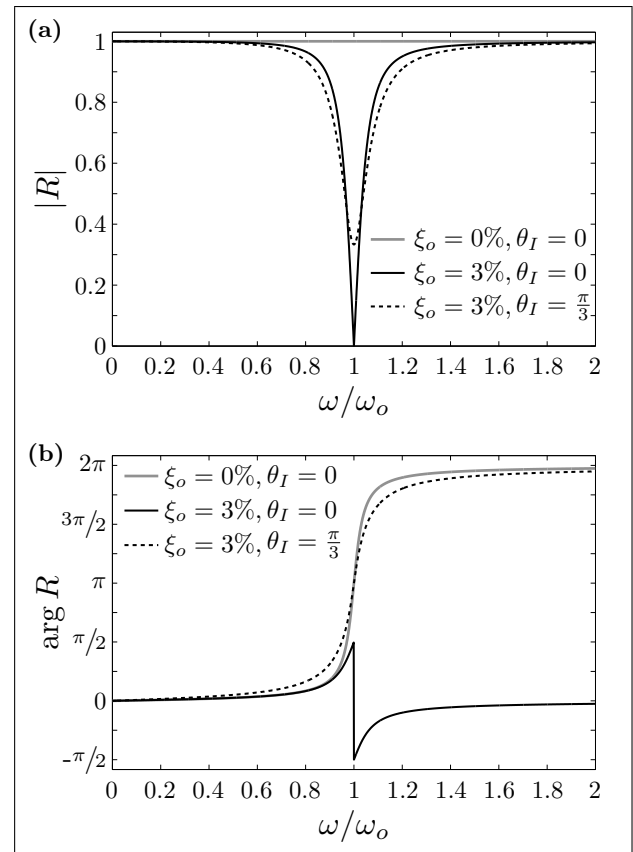


Figure 2. Reflection coefficient of the resonant surface against normalized frequency: (a) amplitude (b) phase. Calculations are performed with $\eta = 6\%$, for various damping ξ_o and angle of incidence θ_I .

4. Experimental validation

Reflective properties of a resonant surface made of Helmholtz resonators are studied experimentally in both impedance tube and anechoic chamber, Figure 3. The design developed in [4] to achieve the scale separation around resonance is used. The resonator consists of a spherical cavity of radius $a = 2 \text{ cm}$, having a circular opening A with diameter $e = 4 \text{ mm}$ and a long straight inner duct with diameter $e = 4 \text{ mm}$ and length $b = 2 \text{ cm}$ (Figure 3(a)). It behaves as a SDOF oscillator with the mass $m_o = \rho_e |A|b$ (air in the duct) and the stiffness $k_o = \gamma P_e |A|^2/V$ (air in the cavity), where $V = 4\pi a^3/3 - |A|b$ is the net volume of the cavity. That provides the theoretical estimate $(2\pi)^{-1} \sqrt{k_o/m_o} \approx 238 \text{ Hz}$ for the eigenfrequency.

Measurements in an impedance tube (*B&K* type 4206, circular cross-section Σ_T , diameter $D = 10 \text{ cm}$) are performed at the University of Salford, U.K. on $N = \{1, 4\}$ resonators secured at the rigid end of the tube with their apertures facing up (Figure 3(b)). A boundary layer analysis (see Section 2) with integration performed over the tube Ω_T (impervious lateral surface) leads to the equivalent admittance condition $\mathbf{v} \cdot \mathbf{n} = \Upsilon_T p_\Gamma$ on Σ_T (analogous to the period) for the propagating waves in the tube, where

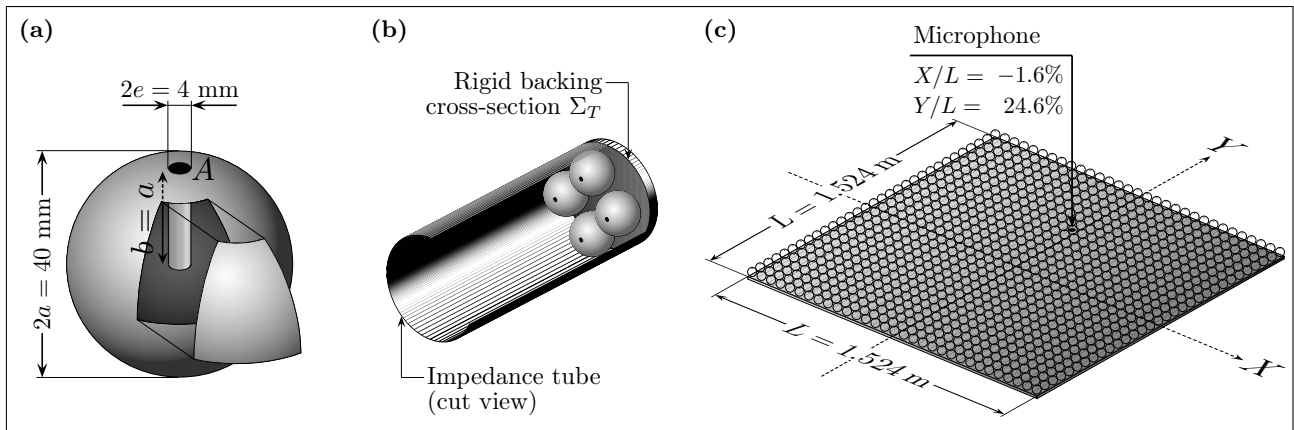


Figure 3. Experimental prototypes. (a) Schematic view of the spherical Helmholtz resonator with details of its inner duct; (b) Arrangement of 4 Helmholtz resonators in the impedance tube; (c) Arrangement of 961 Helmholtz resonators on a rigid surface tested in the anechoic chamber.

$\rho_e c \Upsilon_T = \eta_T F(\omega)$ and $\eta_T = N|A|^2 \rho_e c \omega_o / (k_o |\Sigma_T|) \approx N \times 0.018$. Experiments with a single resonator provide the eigenfrequency $\omega_o/2\pi \approx 253\text{Hz}$ and the damping $\xi_o \approx 6.6\%$ (assessed from the -3dB -bandwidth of the admittance resonance peak) that are used in the analytical model. Results with 4 resonators are shown in Figure 4 and compared with the model predictions. It is confirmed that the resonance leads to a phase shift and a decrease in amplitude of the reflection coefficient (at resonance, the absorption coefficient is $\alpha = 1 - |R|^2 \approx 0.9$). Analogous measurements with 4 non-resonant spheres reveal a nearly-total reflection, as expected. The model is accurate despite the poor scale separation $\epsilon_T = \omega_o D/c \approx 0.46$. Note that the roughness leads to a phase-shift ($< \pi/12 = \mathcal{O}(\epsilon_T)$) neglected in the model at the leading order.

Anechoic chamber measurements are performed at the Open University, U.K. on an array of $31 \times 31 = 961$ Helmholtz resonators (identical to those used in the impedance tube) arranged periodically in a square lattice (spacing $\ell = 5\text{cm}$) on a square rigid board (width $L = 1.524\text{m}$, thickness 12.7mm) with their apertures facing up, see Figure 3(c). The scale separation is satisfied at resonance ($\epsilon_o = \ell \omega_o/c \approx 0.23$) and $\eta \approx 6\%$. The source (*B&K* type 4295) is positioned above the center of the board, at the distance $H = 2.47\text{m}$. The insertion loss $IL = -10 \log |p_\Gamma/p_0|^2$ is shown in Figure 4(c) where p_Γ and p_0 are the pressure recorded at the surface with and without the resonators. As expected, the resonance leads to a sound attenuation at the surface ($IL \approx 3.7\text{ dB}$ at resonance) related to the absorption of the incident field (absorption coefficient $\alpha \approx 0.9$). Since the phase difference between the center and one corner of the board is $[(1 + L^2/2H^2)^{1/2} - 1]H\omega_o/c \approx \pi/3$, the incident field is quasi-plane at the surface. Hence, the data is compared with results presented in Section 3 assuming $\theta_I = 0$. The model predictions

($IL = -10 \log |(1 + R)/2|^2$, where R is given in equation (8)) are in good agreement with the data.

5. Numerical validation

In order to investigate the effect of total absorption predicted by the analytical model in Section 3, a case study is performed using resonators in the form of slotted cylinders. When sufficiently long, they can be modeled as 2D Helmholtz resonators and the Multiple Scattering Theory (MST) can be applied to solve the problem numerically. The case study deals with the reflection of the normally-incident plane wave $P_I = p_I \exp(-i\omega \mathbf{n} \cdot \mathbf{x}/c)$ from a rigid surface Γ upon which the 2D Helmholtz resonators are arranged ℓ -periodically, see Figure 5(a). Resonators (labeled by $j \in \mathbb{Z}$ integer) have a circular cross section with radius $a = 2.5\text{cm}$, a slot facing up with the width $2e = 4\text{mm}$ (angular opening $2\psi = 2e/a$) and the spacing $\ell = 7\text{cm}$. The resonators' center C_j are at the distance $h = 2.7\text{cm}$ from the surface Γ (note $h + a < \ell$).

The boundary of the resonator is rigid, except for the slot where the following conditions are applied: the radial component of the particle velocity is uniform, equal to $v_{\text{slot}} = \Upsilon_o \langle p_{\text{tot}} \rangle$ where $\langle p_{\text{tot}} \rangle$ is the mean pressure over the slot and $\Upsilon_o = Y_o/|A|$ is the slot surface admittance, see equation (7). Its ratio to the air admittance reads $\rho_e c \Upsilon_o = \sigma F(\omega)$ where $\sigma = |A| \rho_e c \omega_o / k_o$. Inside, the Helmholtz resonator has a perimeter-long, 4mm-wide duct wrapped around the cavity, see Figure 5(a). A Finite Element Model provides $\omega_o/2\pi \approx 230\text{Hz}$ and $\sigma = 1.4$ (basic mass-spring analysis provide 250Hz and 1.6 respectively). The design is such that the scale separation is satisfied ($\epsilon_o = \ell \omega_o/c \approx 0.29$) and $\eta = 2e\sigma/\ell \approx 8\%$. A damping $\xi_o = 4\%$ is assumed so that $\eta/2\xi_o = 1$ for the resonant surface to act as an absorbing boundary at resonance, see Section 3.

Following MST procedure (e.g. [5, 9]), the total pressure field is decomposed into $p_{\text{tot}} = P_I + P_R + p_{\text{scat}}$

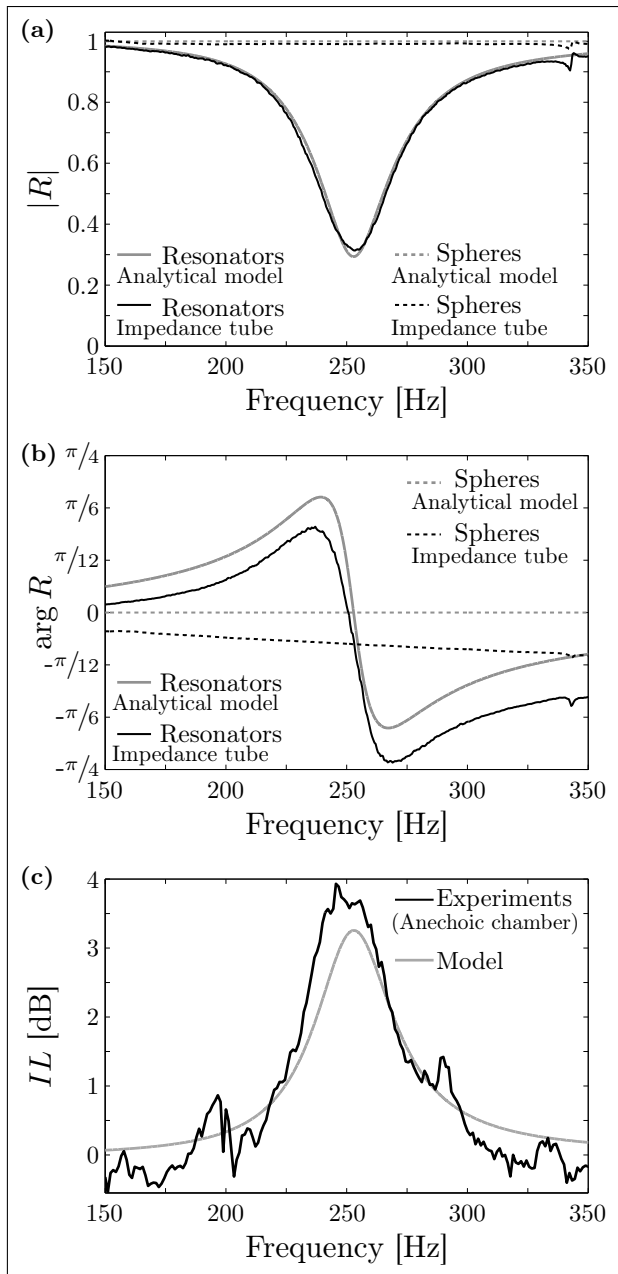


Figure 4. Experimental results compared with the model predictions. (a) amplitude and (b) phase of the reflection coefficient from impedance tube measurements on 4 resonators or 4 non-resonant spheres. (c) Insertion loss from anechoic chamber measurements on 31×31 resonators.

where $P_R = p_I \exp(i\omega \mathbf{n} \cdot \mathbf{x}/c)$ is the field reflected from the rigid surface Γ were the resonators removed and $p_{\text{scat}} = \sum_j (p_j + \tilde{p}_j)$ is the field scattered by the resonators' array: p_j is scattered by the (physical) resonator j and \tilde{p}_j by its mirror-image from the rigid surface Γ . Due to the periodicity, the contributions of all resonators j to the scattered field are equal so that, in the local polar coordinate system (C_j, r_j, θ_j) centered on j (angle θ_j is counted from \mathbf{e}_2):

$$p_j(r_j, \theta_j) = \sum_{n \in \mathbb{Z}} A_n H_n(kr_j) e^{in\theta_j} \quad (9)$$

where H_n is the Hankel function of the first kind and order n and A_n are unknown complex coefficients (independent from j). Because of the mirror-image symmetry, $\tilde{p}_j(\tilde{r}_j, \tilde{\theta}_j) = p_j(\tilde{r}_j, -\tilde{\theta}_j)$ in the polar coordinate system $(\tilde{C}_j, \tilde{r}_j, \tilde{\theta}_j)$ associated with the image-resonator j . The coefficients A_n are found from the boundary conditions applied on a single resonator, say $j = 0$. For that purpose, the fields are (re)expanded in the local coordinate system $(C, r, \theta) = (C_0, r_0, \theta_0)$. Using the Jacobi-Anger expansion [10]:

$$\{P_I + P_R\}(r, \theta) = \sum_{n \in \mathbb{Z}} U_n J_n(kr) e^{in\theta} \quad (10)$$

where $U_n = \{e^{+ikh} + (-1)^n e^{-ikh}\}$ and J_n is the Bessel function of the first kind and order n . Using Graf's addition theorem [10] for resonators $j \neq 0$:

$$p_j(r, \theta) = \sum_{n \in \mathbb{Z}} \sum_{m \in \mathbb{Z}} C_j^{nm} A_m J_n(kr) e^{in\theta} \quad (11)$$

and similarly for $\tilde{p}_j(r, \theta)$ with coefficients \tilde{C}_j^{nm} , where:

$$C_j^{nm} = H_{m-n}(k\sqrt{(j\ell)^2}) e^{i(m-n)(\beta_j + \pi)} \quad (12a)$$

$$\tilde{C}_j^{nm} = H_{m+n}(k\sqrt{(j\ell)^2 + 4h^2}) e^{-i(m+n)\tilde{\beta}_j + im\pi} \quad (12b)$$

and β_j (resp. $\tilde{\beta}_j$) is the angle between \mathbf{e}_2 and CC_j (resp. CC_j). The radial component of the velocity $\mathbf{v}_{\text{tot}} = \mathbf{grad}(p_{\text{tot}})/i\omega\rho_e$ at the boundary $r = a$ is expanded using Fourier decomposition, providing:

$$\frac{\partial}{\partial r} \frac{p_{\text{tot}}}{i\omega\rho_e} \Big|_a = \sum_{n \in \mathbb{Z}} \Upsilon_o \langle p_{\text{tot}} \rangle \frac{\sin(n\psi)}{n\pi} e^{in(\theta - \frac{\pi}{2})} \quad (13)$$

Due to orthogonality, boundary conditions can be formulated separately for each harmonic $e^{in\theta}$. This leads to an infinite system of equations for the unknown coefficients A_n , which is solved numerically by truncation. This gives the pressure $p_{\text{refl}} = P_R + p_{\text{scat}}$ of the wave reflected from the array.

The field p_{refl} is computed above the resonator $j = 0$ (abscissa $x = \mathbf{x} \cdot \mathbf{e}_2 = 0$) and at the distance $z = \{2\ell, 3\ell\}$ above the surface Γ . It is compared in Figure 5(b) and (c) with the analytical model predictions ($p_R = R e^{ikz}$ where R is given in equation (8)). A good agreement between the MST and the analytical model confirms the phenomenon of a nearly total absorption at resonance. A small discrepancy in the phase of the reflected field is due to the surface roughness; a similar discrepancy of the analytical model with measurements has been noted in Section 4.

Finally, the spatial distribution of the pressure p_{refl} is presented in Figure 5(d) at the frequency of resonance and confirms the existence of the periodic boundary layer. In accordance with the analytical model, its amplitude is $\mathcal{O}(\epsilon p_I)$ and it is confined in the close vicinity of the surface array, with characteristic distance of evanescence $\mathcal{O}(\ell)$.

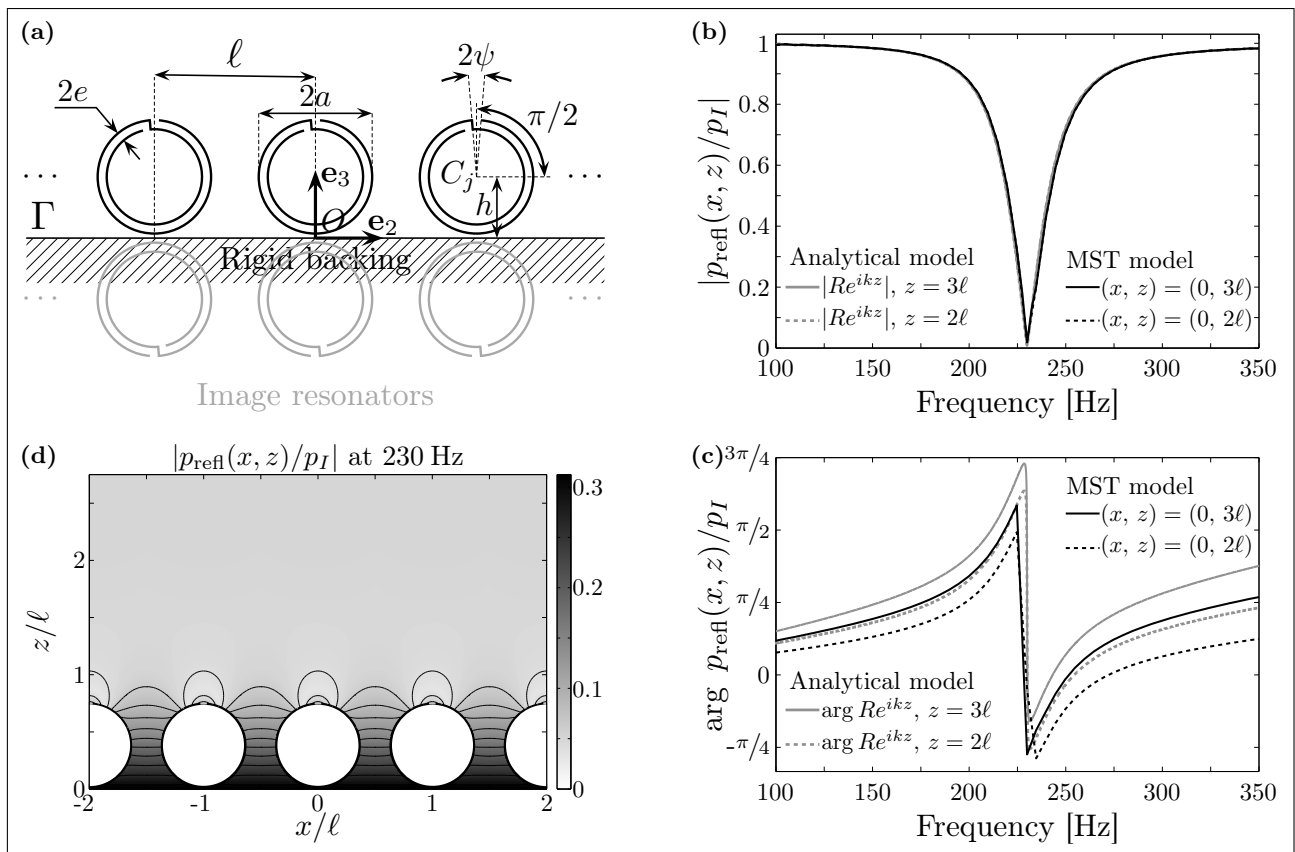


Figure 5. Numerical model in 2D and comparison with the analytical model. (a) geometry of the resonant surface; (b) amplitude and (c) phase of the reflected field at a distance $z = \mathbf{x} \cdot \mathbf{n}$ away from the surface against frequency; (d) spatial distribution of the field reflected from the surface at the frequency of resonance. Fields are normalized to the amplitude p_I of the incident wave.

6. Conclusion

An effective admittance has been derived for a resonant surface with roughness. If a scale separation between the array periodicity and the sound wavelength at resonance is satisfied, the resonant surface can act as an all-pass or a no-pass filter for the reflected field, with a phase-shift around the resonance frequency (crucial to wavefront manipulation [3]). The model has been validated against measurements (absorption coefficient of 0.9 at 253 Hz using 961 Helmholtz resonators) and numerical calculations. It takes account of the multiple interactions, the roughness, the resonators' damping and the angle of incidence at a very low computational cost. It is also applicable to surface waves propagation and more complex arrangements can be made, such as combining oscillators with different eigenfrequencies in a single period.

Acknowledgement

The authors are grateful to A. Tomlinson and P. Seabrook for the help in the experiments. The research has been supported by the U.K. Engineering and Physical Sciences Research Council (grant agreements EP/K037234/1 and EP/K03720X/1).

References

- [1] M. R. Schroeder: Binaural dissimilarity and optimum ceilings for concert halls: More lateral sound diffusion. *J. Acoust. Soc. Am.* 65 (1979) 958-963.
- [2] D.-Y. Maa: Potential of microperforated panel absorber. *J. Acoust. Soc. Am.* 104 (1998) 2861-2866.
- [3] Y. Li et al.: Reflected wavefront manipulation based on ultrathin planar acoustic metasurfaces. *Scientific Reports* 3 (2013) 2546.
- [4] C. Boutin: Acoustics of porous media with inner resonators. *J. Acoust. Soc. Am.* 134 (2013) 4717-4729.
- [5] A. Krynkin et al.: Scattering by coupled resonating elements in air. *J. Phys. D: Appl. Phys.* 44 (2011) 125501.
- [6] E. Sanchez-Palencia: *Non-Homogeneous Media and Vibration Theory. Lectures Notes in Physics*, Vol. 127, Springer-Verlag, Berlin Heidelberg, 1980.
- [7] C. Boutin, P. Roussillon: Wave propagation in presence of oscillators on the free surface. *Int. J. of Eng. Science* 44 (2006) 180-204.
- [8] J.-L. Auriault et al.: *Homogenization of Coupled Phenomena in Heterogeneous Media*. ISTE Ltd and John Wiley & Sons, Inc., 2009.
- [9] A. Krynkin et al.: Acoustic insertion loss due to two dimensional periodic arrays of circular cylinders parallel to a nearby surface. *J. Acoust. Soc. Am.* 130 (2011) 3736-3745.
- [10] H. Bateman, A. Erdelyi (ed.): *Higher Transcendental Functions*, Vol. 2. McGraw-Hill Book Company, 1953.